A hydrophobic gate in an ion channel: the closed state of the nicotinic acetylcholine receptor

To cite this article: Oliver Beckstein and Mark S P Sansom 2006 *Phys. Biol.* **3** 147

INSTITUTE OF PHYSICS PUBLISHING PHYSICAL BIOLOGY

Phys. Biol. **3** (2006) 147–159 doi:10.1088/1478-3975/3/2/007

A hydrophobic gate in an ion channel: the closed state of the nicotinic acetylcholine receptor

Oliver Beckstein[1,2] **and Mark S P Sansom**[2]

[1] The Johns Hopkins University, School of Medicine, Department of Physiology, Biophysics 206, 725 N Wolfe St, Baltimore, MD 21205, USA
[2] Structural Bioinformatics and Computational Biochemistry Unit, Department of Biochemistry, University of Oxford, South Parks Road, Oxford OX1 3QU, UK

E-mail: orbeckst@jhmi.edu and mark.sansom@bioch.ox.ac.uk

Received 2 February 2006
Accepted for publication 14 June 2006
Published 7 July 2006
Online at stacks.iop.org/PhysBio/3/147

Abstract

The nicotinic acetylcholine receptor (nAChR) is the prototypic member of the 'Cys-loop' superfamily of ligand-gated ion channels which mediate synaptic neurotransmission, and whose other members include receptors for glycine, γ-aminobutyric acid and serotonin. Cryo-electron microscopy has yielded a three-dimensional structure of the nAChR in its closed state. However, the exact nature and location of the channel gate remains uncertain. Although the transmembrane pore is constricted close to its center, it is not completely occluded. Rather, the pore has a central hydrophobic zone of radius about 3 Å. Model calculations suggest that such a constriction may form a hydrophobic gate, preventing movement of ions through a channel. We present a detailed and quantitative simulation study of the hydrophobic gating model of the nicotinic receptor, in order to fully evaluate this hypothesis. We demonstrate that the hydrophobic constriction of the nAChR pore indeed forms a closed gate. Potential of mean force (PMF) calculations reveal that the constriction presents a barrier of height about 10 kT to the permeation of sodium ions, placing an upper bound on the closed channel conductance of 0.3 pS. Thus, a 3 Å radius hydrophobic pore can form a functional barrier to the permeation of a 1 Å radius Na^+ ion. Using a united-atom force field for the protein instead of an all-atom one retains the qualitative features but results in differing conductances, showing that the PMF is sensitive to the detailed molecular interactions.

M This article features online multimedia enhancements

1. Introduction

The mechanism of gating of ion channels is a central problem in membrane protein biophysics. One class of channel for which structural and biochemical data are available is the one containing the ligand-gated ion channels (LGIC[3]), represented by the nicotinic acetylcholine receptor (nAChR). This cation-selective channel is made up from five homologous subunits ($\alpha_2\beta\gamma\delta$ in muscle type receptors) packed around a central pore, forming a structure with fivefold pseudo-symmetry [1]. Cryo-electron microscopy studies of the *Torpedo* nAChR [2, 3] have revealed three domains: an extracellular domain containing the neurotransmitter binding site; a transmembrane (TM) domain forming a pore across the lipid bilayer; and an intracellular domain providing binding sites for cytoskeletal proteins (figure 1(*A*)). The structure of the extracellular ligand-binding domain is homologous to that of a water-soluble acetylcholine binding protein [4]. Each subunit of the TM domain contains four

[3] Abbreviations. LGIC, ligand-gated ion channels; nAChR, nicotinic acetylcholine receptor; $5HT_3R$, 5-hydroxytryptamine (serotonin) receptor; $GABA_{A,C}R$, γ-aminobutyric acid receptor type A or C; GlyR, glycine receptor; ACh, acetylcholine; gA, gramicidin A; cryo-EM, cryo-electron microscopy; TM, transmembrane; MD, molecular dynamics; PMF, potential of mean force; WHAM, weighted histogram analysis method; MscS, mechanosensitive channel of small conductance.

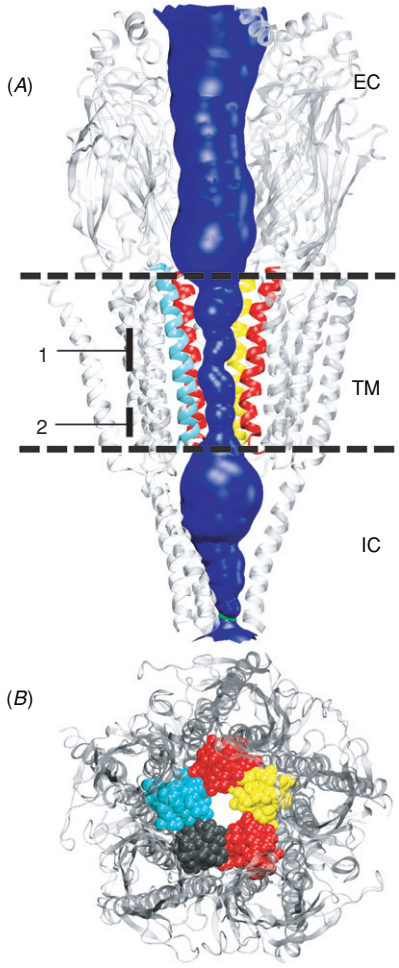

Figure 1. (*A*) Overall architecture of the nAChR (PDB id 2BG9) as determined by cryo-electron microscopy [3], showing the extracellular (EC), transmembrane (TM) and intracellular (IC) domains and the surface of the pore (calculated with HOLE [7]). The position of the gate is currently intensely debated, with some evidence pointing to the region of the hydrophobic girdle (1) and other experiments indicating the constriction close to the intracellular domain (2). The horizontal lines indicate the approximate location of the lipid bilayer. The M2 helices are colored by subunit: α (red), γ (yellow), δ (cyan); the β subunit is omitted for clarity but shown in black in the top view below. (*B*) Structure of the nAChR TM domain viewed down the pore axis from the extracellular end, with the M2 helices in space-filling format (images produced with VMD [8] and RASTER3D [9]).

membrane-spanning helices, M1 to M4. The five M2 helices come together to form an approximately symmetrical TM pore (figure 1(*B*)). The lower (intracellular) half of the pore is formed by a polar 3 Å constriction (lined by serine and threonine residues), whilst the upper (extracellular) half of the pore contains a more hydrophobic constriction of the same radius, lined mainly by valine and leucine residues. The protein was crystallized in the absence of acetylcholine; thus the receptor is presumed to be in a functionally closed state. Despite this, the narrowest zone of the pore is sufficiently wide to accommodate e.g. three water molecules or a Na^+ ion and two water molecules side by side. Thus, there is an

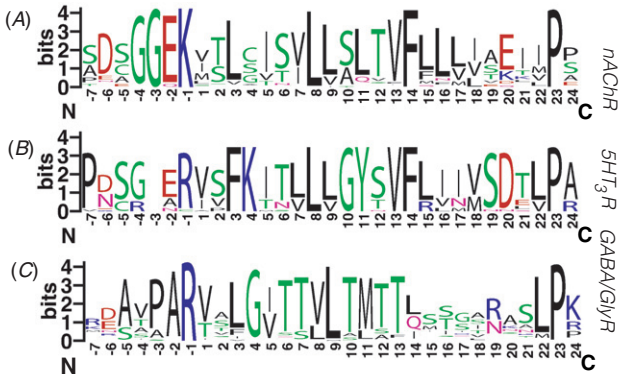

Figure 2. Sequence logos [20] for the ligand gated ion channels in the M2 region. (*A*) nAChR, (*B*) $5HT_3$ (serotonin) receptors, (*C*) GABA and glycine receptors. Acidic residues are marked red, basic ones blue, polar ones green. Hydrophobic residues (and proline) are colored black. Residues are counted within M2, using the 'prime' nomenclature where αM243 is designated 1′. The information content per residue is measured in bits; a totally conserved residue has an information content of 4.32 bits. The size of a letter indicates this amino acid's contribution to the information content at the position.

apparent paradox of a functionally closed pore which is not fully occluded. This contrasts with e.g. the structure of the bacterial K^+ channel KirBac1.1 [5] where the putative gate has a radius of 0.5 Å, thus sterically occluding the ion passageway. However, the situation is already less clear-cut for KcsA [6], another bacterial K channel, whose gate constriction is just wide enough to admit a bare potassium ion. Interestingly, those constrictions are also formed by hydrophobic residues.

A possible answer to the paradox lies in the concept of the *hydrophobic gating* of ion channels, which has been postulated in the literature [10–14] and was quantitatively developed on the basis of computer simulations of simplified pore models [15–17]. A hydrophobic gate is a constriction that acts as a desolvation barrier for ions. It is so narrow (pore radius $R < 4$ Å) that an ion has to shed at least some water molecules from its hydration shell in order to pass the constriction. Because this requires a large amount of free energy (the solvation free energy for a potassium ion is about -308 kJ mol^{-1} and for a sodium ion it is -391 kJ mol^{-1} [18]), passage of the ion is energetically unfavorable and thus blocked, even though the geometry would permit permeation of a partially hydrated ion or a water molecule. The desolvation barrier is only effective if hydration shell water molecules cannot be temporarily substituted with e.g. hydroxyl groups from side chains or the protein backbone as seen, for instance, in the narrow ($R \approx 1.5$ Å) selectivity filter of K channels [6, 19]. Thus, the constriction has to be lined by hydrophobic side chains, whose methyl groups will not participate in solvating an ion. According to the electron microscopy structure [2] and biochemical studies [21, 22], the central portion of the nAChR pore is lined by valine and leucine side chains. Analysis of Cys-loop receptor M2 sequences in terms of sequence logos [20], shown in figure 2, reveals that the LxxxVxxxV/L motif is well conserved amongst nAChR receptors (residues 9′, 13′ and 17′ when numbered from the N-terminal end of the M2 helix),

and is replaced by an equivalent LxxxVxxxI motif in $5HT_3$ receptors [21, 23–25], hinting at the biological importance of these hydrophobic residues. There is also evidence that a similar motif is conserved in prokaryotic homologues of the nAChR [26], suggesting that this was an early evolutionary feature of this family of ion channels. Here we argue that these hydrophobic residues form a *hydrophobic gate* (called the 'hydrophobic girdle' by White and Cohen [10] and later Unwin and colleagues [2, 11]). In GABA and glycine receptors the LxxxVxxxV/L motif is replaced by a LxxxT motif (residues 9′ and 13′), suggesting that the nature of the gate may be modified in anion-selective channels.

However, the position of the gate is highly contentious, with different experiments pointing toward different locations (see figure 1). As discussed below, some studies employing methods probing the accessibility of pore lining residues find the gate close to the intracellular end of the pore [22, 27–30] whereas the EM structure [2] and the same accessibility method applied to $5HT_3R$ [31] point to the hydrophobic girdle as the gate; other mutation studies in LGIC point to the importance of the ring of conserved Leu and Val residues, suggesting a gate closer to the extracellular end of the pore [25, 32–36]. Knowing the position of the gate is crucial in the larger enterprise of understanding the full gating behavior of the ligand gated ion channels as a paradigm for a complex receptor structure-function relationship [37]. The simulations presented in this work are answering the question whether a hydrophobic girdle (as seen in the EM structure) could act as a barrier to ion permeation and provide quantitative evidence for the qualitative idea of a hydrophobic gate.

For the bacterial mechanosensitive channel MscS, the concept of hydrophobic gating has already been investigated using molecular dynamics computer simulations. Anishkin and Sukharev [38] conclude that the crystal structure, which exhibits a hydrophobic constriction of radius 4 Å [39], represents a closed state because water (and ions) do not enter the putative gate; Spronk *et al* [40] challenge this view because in their simulations both ion and water fill the pore once an external transmembrane potential is applied across the channel. Continuum electrostatics calculations on a simplified model of KcsA [12] and the crystal structure [41, 42] indicate that the intracellular hydrophobic constriction presents a high dielectric barrier even though it does not sterically occlude the ion pathway. Recent continuum electrostatics [43] and short equilibrium MD and Brownian dynamics calculations [44] suggest that hydrophobic gating may also apply to nAChR. However, comparisons with estimates of free energy profiles for ion permeation through model pores based on atomistic simulations [17] showed that continuum approximations can be inaccurate for pores of sub-nanometer dimensions, especially when hydrophobic effects (which are collective effects of the solvent) are involved. Thus, such methods cannot readily provide a rigorous test of the hydrophobic gating hypothesis. Furthermore, equilibrium simulations can only show what would happen under equilibrium conditions within the time span of the simulation (i.e. 1–100 ns, this time scale still being perhaps three orders of magnitude short of that of channel gating). For instance, for an *open* state conductance of 50 pS as typical for nAChR [13] one would expect on average about one ion permeation event per about 60 ns in equilibrium (using rate theory to estimate the equilibrium flux: start from the rate theory flux $\Phi = I/q \approx \Phi_0 \sinh(qV/2kT)$ [16], expand near equilibrium, i.e. vanishing driving potential $qV \ll kT$, and using $I = gV$ arrive at a rough estimate for the equilibrium flux $\Phi_0 \approx 2kTgq^{-2} = 0.016\,\mathrm{ns}^{-1}$ or one ion per 63 ns). For a *closed* gate the time for such an event to occur would be at least one order of magnitude larger. This means that it is impossible to quantify any sizable energy barriers, such as that in a closed gate, using straightforward equilibrium MD. In order to probe such a region, i.e. to estimate reliably the height and extent of the energy barrier to ion permeation in the nAChR pore, and thus to test the hydrophobic gating hypothesis, detailed atomistic free energy calculations are required. Although those 'potential of mean force' calculations are computationally expensive, there are a number of comparable simulations that have been used to determine quantitatively the energy landscape experienced by K^+ ions within the selectivity filter of KcsA [19] and the gramicidin A (gA) pore [45–47].

We present the results of such calculations for the height of the energetic barrier associated with the closed gate of the nAChR, and show that they support the hydrophobic gating hypothesis. Furthermore, we evaluate the robustness of this conclusion in relation to the forcefield employed. These results demonstrate the value of a theoretical physical approach to a mechanistic biological problem that is difficult to address via direct experimentation.

2. Methods

In order to determine the equilibrium distribution and the potentials of mean force of water and ions within the pore of the nAChR, we employed fully atomistic molecular dynamics simulations of the pore-forming M2 helix bundle, embedded within a membrane-mimetic slab of methane-like pseudo-atoms, with water and ions (Na^+ and Cl^-) equivalent to a concentration of 1.3 M on either side of the slab (figure 3).

2.1. Model

The initial model of the M2 bundle consists of residues αE241 to αV271 (and corresponding residues on the other chains) from the 4 Å resolution cryo-EM structure (PDB id 1OED [2]). All titratable residues are in their default (charged) state at pH 7 (as predicted by pK_a calculations on the whole TM domain using WHATIF [48, 49] with DELPHI [50] as the Poisson–Boltzmann solver) except for the helix termini, which were kept neutral to minimize their influence on the system. The M2 bundle is embedded in a bilayer-mimetic slab of thickness 3.2 nm, made from CH_4 molecules, which are held on a face-centered cubic lattice (cubic lattice constant 0.75 nm) by harmonic restraints of strength $k_0 = 1000\,\mathrm{kJ\,mol^{-1}\,nm^{-2}}$. The total system size was 15 298 atoms, made up of 2819 protein atoms, 2974 water molecules, 689 'membrane' CH_4 molecules and 112 ions. The pore was initially solvated with water. Cations and anions were added alternately by

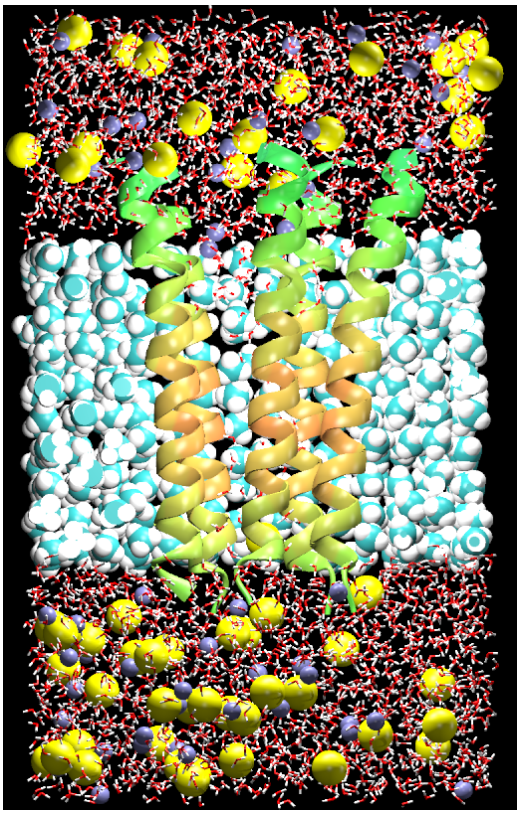

Figure 3. Simulation system. The M2 helix bundle is depicted as ribbons (from the cryo-electron microscopy structure of the nAChR TM domain, pdb 1OED [2]), the membrane mimetic slab is made from methane molecules on a face-centered cubic lattice, water molecules are represented as sticks, and ions as ice-blue (Na^+) or yellow (Cl^-) spheres.

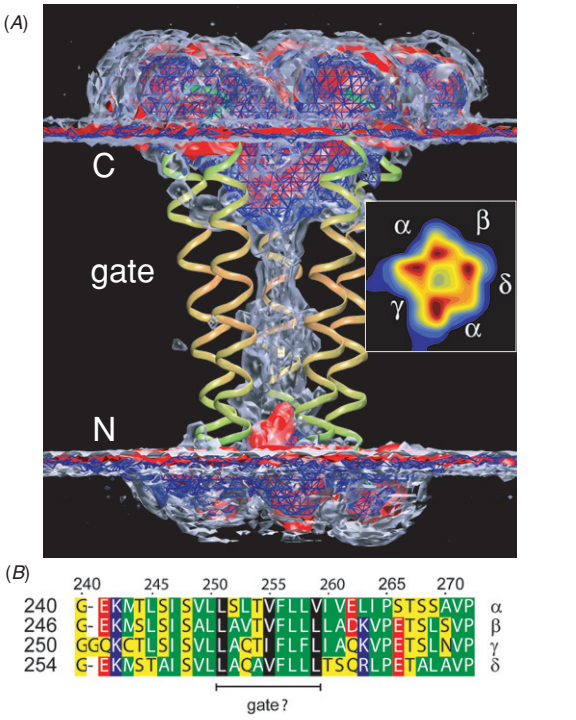

Figure 4. (*A*) Water and spatial ion densities in the nAChR M2 helix bundle (ribbons; the membrane mimetic slab is omitted for clarity). The N and C termini of the helices (corresponding to the intracellular and extracellular ends of the transbilayer pore respectively) and the hydrophobic gate are labeled. The three surfaces show the average density of water molecules (gray surface, contoured at 95% of the bulk density), sodium ions (blue surface), and chloride ions (red surface), both contoured at 0.1 M. These are taken from a 60 ns simulation on the M2 helix bundle embedded in a membrane-mimetic slab and bathed in a 1.3 M NaCl solution. The inset shows a cross-section through the water density in the region of the gate. The water density is contoured on a color scale, ranging from 5% (deep blue) to 140% (deep red) of bulk density.
(*B*) Sequence alignment for the M2 helix sequences from the four subunit types of the *Torpedo* nAChR. The putative hydrophobic gate region, extending from L251 to V259 of the subunit, is indicated below the sequence alignment.

exchanging a water molecule at the position of minimum potential energy for the ion, leading to an approximately uniform distribution of ions. For the protein and CH_4 the OPLS all-atom force field [51] was used, but for a sensitivity analysis we also performed simulations with the united-atom GROMOS96 force field [52]. For water the SPC model was employed [53], and ion parameters were taken from the work of Åqvist [54]. During the simulations, the protein backbone was harmonically restrained with force constant k_0 whilst the side chain atoms, water and ions were free to move, resulting in positional root mean square fluctuations (average C_α fluctuation 0.3 Å) similar to those seen in simulations of the TM helix bundle in a lipid bilayer [55] (about 0.6 Å, excluding mobile loops).

2.2. Simulation details

Simulations were performed with GROMACS 3.2.1 [56] at constant temperature (300 K or 27 °C) and pressure (1 bar) normal to the membrane, using weak temperature (time constant $\tau = 0.1$ ps) and pressure coupling ($\tau = 1$ ps) algorithms. Electrostatic interactions were accounted for by a particle mesh Ewald method [57] (real space cutoff 1 nm, grid spacing 0.15 nm, fourth order interpolation), whereas van der Waals interactions were computed within a cutoff of 1.4 nm. Protein bonds were constrained with the LINCS algorithm [58] whereas the SPC water molecule bonds were constrained with SETTLE [59]. The MD time step was 2 fs.

The equilibrium simulation in the OPLS-AA force field was performed for 60 ns; GROMOS96 equilibrium simulations were run for 80 ns. The single-channel conductance under physiological conditions of the (open) *Torpedo* nAChR is 30–50 pS [13], corresponding to an equilibrium mean passage time per ion of about 60 ns. Thus, as mentioned in the introduction, a 60 ns simulation should enable us to sample the distribution of ions within an M2 bundle pore if it were permeable to ions (though in any case one would not expect to observe permeation events).

Potentials of mean force. Potentials of mean force (PMF) for permeant species were obtained from a combination of equilibrium and umbrella sampling [60, 61] simulations. A

starting configuration for each umbrella window was obtained from the equilibrium simulation by selecting a frame from the trajectory that had a particle of interest within about 1 Å of the window center, or by exchanging a suitable water molecule with an ion. Thus neighboring window configurations tend not to be correlated. For umbrella sampling, the particle of interest was harmonically restrained to subsequent positions on the channel axis (with typical values of the restraining force constant 1558 kJ mol^{-1} nm^{-2}) in 101 or more windows of width $\Delta z = 0.396$ Å for Na^+, Cl^-, and water (see table S1 in the supplementary data available at stacks.iop.org/PhysBio/3/147 for a detailed listing of umbrella sampling parameters). This choice of umbrella sampling parameters allows the particle of interest to diffuse into neighboring windows (the energy required to do so is only about 1.5 kT, i.e. a typical thermal fluctuation), leading to good overlap between windows [45]. Each window simulation was typically run for 1.2 ns, with the initial 0.2 ns being discarded as equilibration time; hence a single PMF comprises 101 ns of simulation time or about 50 million configurations of the sampled particle (at a simulation time step of 2 fs). The umbrella sampling simulations for Na^+ with the OPLS force field were extended into the bulk regions with a harmonic flat-bottomed cylindrical confinement potential [46] (radius 1.3 nm, force constant 4500 kJ mol^{-1} nm^{-2}). 25 windows were added on the intracellular side ($\Delta z = 0.4$ Å, $k = 1527$ kJ mol^{-1} nm^{-2}) and 20 on the extracellular side ($\Delta z = 0.5$ Å, $k = 977$ kJ mol^{-1} nm^{-2}), so that the Na^+ PMF comprises of 146 windows over a length of 60 Å.

Resulting histograms were unbiased using the weighted histogram analysis method [62] (WHAM), with 300–500 bins and a tolerance of 10^{-5} kT for the individual window offsets. The PMFs are converged with respect to the number of bins and the tolerance; more details can be found in the supplementary data available at stacks.iop.org/PhysBio/3/147. PMFs were constructed from matching the umbrella-sampled PMF to the PMF derived from the equilibrium density (i.e. the Boltzmann-sampled PMF)

$$G(z) = -kT \ln \frac{n(z)}{n_0} + C \qquad (1)$$

in the mouth regions of the pore ($n(z)$ denoting the average density in the pore along the z-axis and n_0 the density in the bulk, C being an undetermined constant not relevant for our discussion). Both methods produce overlapping results in the mouth region, even though combining them is not a rigorously defined operation (see below).

Many ion channel properties are discussed in terms of the one-dimensional PMF along a single reaction coordinate (also referred to as the free energy profile) [13]. However, as Roux *et al* [63] point out, there are a number of theoretical/conceptual and practical problems associated with the free energy profile. It is only well defined in the pore region because in the bulk the motion of the particle is not bounded orthogonal to the reaction coordinate (although in MD simulations periodic boundary conditions ensure artificial confinement). Practically, one can umbrella-sample into the bulk/mouth regions with the help of a cylindrical confinement potential. This procedure was employed for the OPLS Na^+ PMF and resulted in a better converged PMF. On the practical side, one cannot hope to sample the full multi-ion PMF because all movements of ions are 'slow' degrees of freedom. With a 1D reaction coordinate approach only one slow degree of freedom (such as the movement in z-direction) can be controlled; the other slow degrees will not equilibrate on the time scale of the umbrella sampling simulation and therefore should be controlled by other means (see [63] for a full discussion). A well-defined quantity is the one-ion PMF, which is obtained as the PMF of one particular ion while no other ions are present in the pore. From the one-ion PMF one can, for instance, compute the maximum single channel conductance, equation 2. If the other ions are not excluded from the pore by a computational device such as an exclusion potential [45, 47] one can resort to only including those frames of a trajectory in the WHAM analysis during which the one-ion condition is fulfilled. The latter approach was chosen for the OPLS Na^+ PMF. The one-ion region $\mathcal{P}_1$ was defined as $-21.6\,\text{Å} \leqslant z \leqslant 6.4\,\text{Å}$ (roughly corresponding to the region between the 1′ and the 17′ positions; see figures 5 and 7) on the basis that the ionic equilibrium densities (figure 5) drop sharply inside this region and, that after analysis of umbrella windows, only 14 out of 72 windows showed multiple ion occupancies in this region. Those windows were simply rerun after exchanging the offending ion(s) with a bulk water or after assigning new initial velocities. Both approaches yielded simulations with only the sampled ion in $\mathcal{P}_1$. (Details can be found in the supplementary data available at stacks.iop.org/PhysBio/3/147.)

We also calculated a PMF across the whole pore by including the additional windows outside $\mathcal{P}_1$. Although this is not a rigorous approach, it turns out that including the multiple-occupancy regions in the WHAM procedure does not alter the one-ion part of the PMF. Because WHAM is a rather sensitive 'global' fitting procedure this gives at least an indication that our PMFs are reasonably robust quantities, even without the full rigorous treatment. The Boltzmann-sampled PMF is by definition the multi-ion PMF (though it might not be converged); our umbrella-sampled PMF contains multi-ion components in the mouth region and the one-ion PMF in $\mathcal{P}_1$. We join those two PMFs because they tend to overlap rather well in the mouth regions of the pore and because the umbrella-sampled PMF for water superimposes almost exactly on the Boltzmann-sampled one (which can easily be sampled across the whole pore) as shown in figure 7.

2.3. Analysis

Simulations. Pore radius profiles were calculated with HOLE [7] from the cryo-EM structure with a probe radius of 0.14 nm.

To address the question of the existence of a vapor-lock mechanism we analyzed the water occupancy N_{water} of the hydrophobic constriction (at 13′, $-2.6\,\text{Å} \leqslant z \leqslant 1.6\,\text{A}$, see figures 5 and 7) from the 60 ns equilibrium simulation. This region was chosen after preliminary inspection showed intermittent vapor phases only occurring in this 4.2 Å section of the pore, reminiscent of results from our previous work on hydrophobic model pores [15, 64].

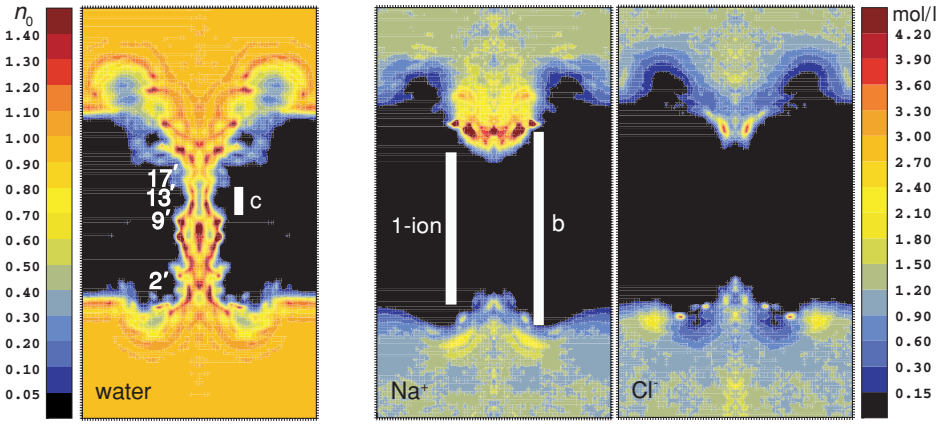

Figure 5. Radially averaged density of water, Na^+, and Cl^- in the M2 pore of nAChR (mirrored at the z-axis to give an impression of the pore environment). Data averaged over one 60 ns equilibrium simulation. Water density is given as a fraction of the bulk density of SPC water ($n_0 = 0.9669\,\mathrm{g\,cm^{-3}}$) and the ionic density as a concentration. The position of the residues forming the hydrophobic girdle (9′, 13′, 17′) and the 2′ position (at the intracellular constriction) are indicated. The white bars define regions of the pore mentioned in the text (c: 13′ hydrophobic constriction, 1-ion: region from which a true 1-ion PMF was obtained, b: barrier region).

Single-channel conductances were estimated from the PMF $G(z)$ as [46, 63]

$$g_{\max} = \frac{e^2}{kTL^2}\left(L^{-1}\int_{\mathcal{P}_1} \mathrm{d}z\, D(z)^{-1}\,\mathrm{e}^{+G(z)/kT}\right)^{-1} \times \left(L^{-1}\int_{\mathcal{P}_1} \mathrm{d}z\,\mathrm{e}^{-G(z)/kT}\right)^{-1} \quad (2)$$

where the averages are carried out over the pore region $\mathcal{P}_1$ where only one ion occupies the pore. The diffusion coefficients in the pore were estimated to be half of the experimental bulk value [65] (D_{bulk} (Na^+) $= 1.33\,\mathrm{nm^2\,ns^{-1}}$, D_{bulk} (Cl^-) $= 2.03\,\mathrm{nm^2\,ns^{-1}}$ [13]). This $g_{\max}$ estimate is strictly true only for one-ion channels (or one-ion PMFs). In addition to $\mathcal{P}_1$ we also define the barrier region $\mathcal{P}_b$, $-23\,\text{Å} \leqslant z \leqslant 10\,\text{Å}$ (E−2′ to E20′), which is the extent of the barrier in the Na^+ PMF (see figure 7). The one-ion condition is not strictly fulfilled but because of the robustness of the one-ion PMF we use the PMF over $\mathcal{P}_B$ as an approximation for the proper one-ion PMF and calculate $g_{\max}$ across the full barrier. (Because $g_{\max}$ depends on L^{-2} we use the exact same definition for the pore regions for all our simulations in order to compare the conductance estimates.)

Sequences. An alignment of the transmembrane domain of the ligand gated ion channels was prepared, based on the Pfam ('protein family') PF02932 (neurotransmitter-gated ion-channel transmembrane region), which contains 616 members (version 14.0 of Pfam [66]). After removal of fragmentary sequences, 511 remained, which were aligned with ClustalW [67]. A calculation of an average-distance neighbor joining tree (using JalView [68]) shows four distinct families (nAChR, $5HT_3R$, $GABA_AR$, GlyR) for the whole alignment. Focusing on the M2 region three distinct families remain: cation-selective nAChR (234 sequences) and $5HT_3R$ (20 sequences), and anion-selective GABA/GlyR (244 sequences). From the M2 sequences, 'sequence logos' [20] were created.

3. Results and discussion

The long 60 ns equilibrium simulation reveals that although water penetrates the full length of the pore, ions do not (figures 4(*A*) and 5). Instead there is a local increase (up to 6×) in the concentration of cations at the extracellular mouth of the pore. This reflects the presence of rings of negatively charged aspartate and glutamate residues at the mouths of the M2 helix bundle (at the 20′ and 24′ positions), as can be seen in figures 4(*B*) and 2. By increasing the local ion concentration near the channel entrance, the charged rings lower the effective access resistance and so increase the single-channel current once the pore opens [13].

Ions fail to enter the central hydrophobic section of the M2 pore: at a bulk concentration of 1.3 M NaCl, the ionic density in the gate drops to less than 0.1 M during 60 ns of equilibrium MD. This is consistent with the hydrophobic gating hypothesis. However, a 60 ns duration equilibrium simulation cannot sample the distribution of ions over an energy barrier of greater than about $5\,kT$ reliably. Thus, umbrella sampling simulations are needed to estimate the barrier height and exact position of the residues responsible for the barrier (see below).

3.1. Water in the hydrophobic constriction

The presence of the peptide backbone makes the nAChR pore significantly more polar than hydrophobic model pores studied in our previous simulations [16, 17, 64]. It is, therefore, not surprising that water is seen all along the pore (figure 5). The putative gate region around αV13′ (region c in figure 5) is of particular interest, in that the water density is localized in an approximately pentameric arrangement, forming a hollow tube with, on average, little water in the center (inset of figure 4(*A*)). This hints at strong constraints on water positions: water may only maintain its presence if it interacts in a fairly restricted configuration. Inspection of the trajectory reveals that the pentameric distribution only emerges on averaging. It does not reflect structures such

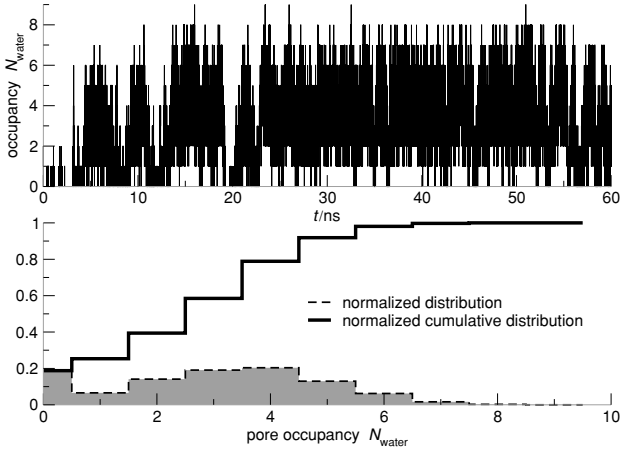

Figure 6. *Top*: number of water molecules N_{water} in the hydrophobic constriction at the 13′ position (pore occupancy) over a 60 ns equilibrium simulation. *Bottom*: normalized distribution of the pore occupancy and its cumulative distribution.

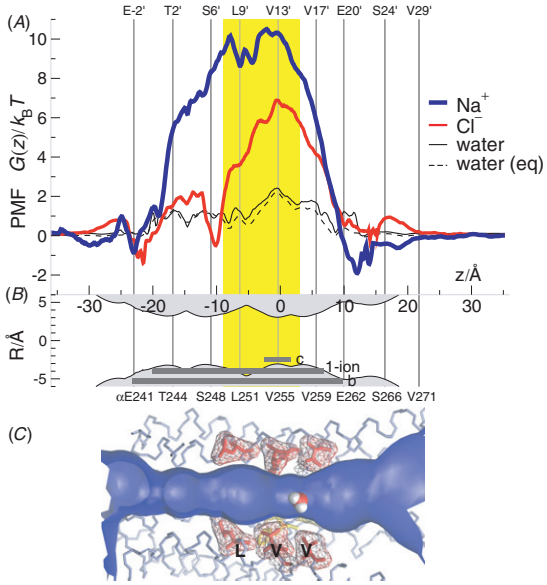

Figure 7. Free energy and radius profiles of the M2 bundle pore. (*A*) Potentials of mean force (PMFs) for water (black line), Cl^- (red line), and Na^+ (blue line) along the z axis of the M2 pore (from umbrella-sampled simulations). The dashed line is the PMF for a water molecule in the pore, derived from the density of one 60 ns equilibrium simulation (equation 1). The intracellular end of the M2 pore is at $z \approx -25$ Å and the extracellular end is at $z \approx +15$ Å. The putative gate region runs from ≈ -9 Å to +5 Å (marked by the yellow band). (*B*) The HOLE pore radius profile along the z axis. The sequence numbering at the top of (*A*) is using the 'prime' nomenclature commonly applied to M2; the equivalent residue numbers in the *Torpedo* subunit sequence are given below (*B*). Gray bars indicate the same pore regions as in figure 5 (c: hydrophobic constriction, 1-ion: region with true 1-ion PMF, b: barrier region). (*C*) The pore lining surface, scaled and aligned so it corresponds to the pore profiles in (*A*) and (*B*). The side chains of residues corresponding to L251, V255 and V259 of the α subunit are shown, as is a water molecule (for purposes of comparison only) in space-filling format within the pore.

as highly ordered five-membered rings. On occasions, a hydrogen-bonded string of water molecules can be seen to sample the preferred locations, although mostly the pore is simply water filled (also see figure S4 and the movie available at stacks.iop.org/PhysBio/3/147). In MD simulations of water in MscS, extended vapor phases with some intermittent water filling were observed in the putative gate region [38, 40, 69]. Partly on this basis, Anishkin and Sukharev [38] concluded that the MscS structure represents a closed state and hypothesized that a similar 'vapor-lock' mechanism might be at work in nAChR. As figure 6 shows, the number of water molecules in the constriction fluctuates between zero and nine over 60 ns. For 75% of the time, the hydrophobic constriction is filled with two to nine water molecules and for 19% it is void of water (and as such our results are more similar to what Sotomayor and Schulten [69] found for water in the MscS hydrophobic constriction). The distribution in the lower panel of figure 6 resembles data obtained for hydrophobic model pores [64]; in particular, it is bi-modal with a meta-stable vapor-like state ($N_{water} = 0$) and a stable liquid-like state ($N_{water} > 1$). (In the supplementary data available at stacks.iop.org/PhysBio/3/147 we discuss the hydrophobic constriction as a simple hydrophobic nano pore.) These data indicate that extended vapor phases are not responsible for blocking ionic current, simply because those phases are not sufficiently stable. Nevertheless, the appearance of a vapor state is an indicator of the hydrophobic nature of the pore, which, as we will demonstrate below, in itself can already be sufficient to create a desolvation barrier for Na^+.

3.2. Position of the gate

From the water equilibrium distribution it is possible to estimate (via a Boltzmann transformation, equation (1)) a free energy profile (i.e. PMF) for water along the pore axis. This direct estimate coincides exceptionally well with the PMF obtained by umbrella sampling (see figure 7(*A*)). Water molecules do not encounter significant barriers (the highest one is $2kT$ at the central residue αV255 of the hydrophobic girdle), again indicating that the closed-state nAChR pore is largely water filled. Because a vapor-lock mechanism of gating does not seem to be an accurate description, a more detailed investigation of the energetics of ion permeation such as the full PMFs of the ions is required.

The same umbrella sampling procedure can be used to obtain PMFs for ions (both Na^+ and Cl^-) along the pore axis (figure 7(*A*)). Na^+ ions encounter a significant barrier of about 10.5 kT. An estimate of the single-channel conductance for Na^+, based on the PMF (equation 2), yields $g_{max} = 0.33$ pS (table 1). This is much lower than the experimentally observed open state conductance of 30 pS to 50 pS [13]. In fact, the conductance for the whole channel would be even smaller as our estimate does not include the resistance encountered in other regions of the receptor and the access resistance at the mouths [70]. As our computed g_{gmax} for sodium, which is an upper bound on the true single channel conductance, is already much smaller than the (experimental) open state conductance we conclude that the M2 pore appears impermeable to Na^+ and hence represents a closed conformation. The barrier

Table 1. Maximum single channel conductance estimates, calculated with equation (2) over the region indicated in the table. Throughout the text the value across the whole *barrier* region $\mathcal{P}_B$ is quoted but the *1-ion* region $\mathcal{P}_1$ value is also given for comparison. k_{bb} denotes the strength of the backbone restraints on the backbone of the M2 helices; $k_0 = 1000$ kJ mol^{-1} nm^{-2}.

			g_{max} (pS)	
Force field	k_{bb}/k_0	Ion	Barrier	1-ion
OPLS-AA	1.0	Na^+	0.33	1.0
		Cl^-	21	37
GROMOS96	1.0	Na^+	18	108
		Cl^-	11	25
GROMOS96	0.2	Na^+	16	87

for sodium is wide, ranging over the complete length of the hydrophobic girdle, which we identify with the gate. Thus, the hydrophobic gate may be thought of as being *distributed* from the αL251 to the αV259 side chain rings. The peak of the barrier coincides with a very narrow (radius 3 Å—see figure 7(*C*)) and hydrophobic (αV255) region of the pore but the width of the barrier is mainly due to αL251, which lines the central part of the nAChR pore.

A previous study computed Poisson–Boltzmann continuum electrostatic solvation free energy profiles across the nAChR gate region (using the full transmembrane domain) in order to assess the influence of changing pore geometry on ion transport properties [55]. For the cryo-EM-like configuration the results differ somewhat from the fully atomistic, explicit solvent PMF (figure 7(*A*)). Notably, the solvation free energy profile shows three peaks at S248, L251 and V255, with the V255 peak being the smallest. This discrepancy is not surprising and rather points to the inherent (and well known [63, 71]) limitations of the continuum approach, namely a very strong dependence on small pore radii (which will dominate the result if computed from a single structure), and the omission of hydrophobic destabilization of the solvent in apolar regions [16].

Chloride ions encounter a less pronounced barrier of about 6.5 kT, which is also peaked at the hydrophobic girdle. In the case of the Cl^- PMF shown in figure 7(*A*) the upper-bound estimate on g_{max} is rather large with a value of 21 pS (table 1) because the barriers are not very high and not very wide. According to the PMF, the central cavity (formed mainly by L9′) can stabilize a solvated Cl^- ion but not a solvated Na^+. It is somewhat surprising that the negatively charged rings (20′ and 24′, called the extracellular ring [72]) do not contribute to any appreciable barrier for Cl^- even though one might expect strong repulsion between anions and the negatively charged glutamates or aspartates. The simulations show that all the negative charge ($-6e$) is effectively screened by Na^+ ions (figure 5) so that, on average, the ions form a double layer protruding into the mouth region, with a cloud of cations enveloping the anions as shown by the 3D density in figure 4(*A*). This picture is consistent with the fact that charge selectivity is not conferred by the extracellular ring but rather by the so-called intermediate ring at $-2'$ [72–75]. The PMF, however, does not exhibit a barrier near $-2'$. This is due to the fact that we truncated our model at $-2'$ and that the whole intracellular domain of nAChR is missing from our model. Selectivity requires charged groups protruding into a confined environment [76] but the $-2'$ residues are exposed to the bulk in our simulations so that their effect is effectively screened. It should also be noted that the Cl^- PMF was constructed from umbrella windows that included multi-ion configurations in the pore, and hence does not constitute a true one-ion PMF. Judging from the analysis of the Na^+ PMF the difference is unlikely to be more than a moderate increase in barrier height by 1 to $2kT$.

Allen *et al* [47] suggest a number of corrections to fully atomistic PMFs, which include the effect of polarization of the surrounding lipid hydrocarbon chains and a correction for the finite (but periodic) system size. In the case of gA, those corrections lowered the PMF by a few kT [46, 47]. An additional source of uncertainty is the absence of the outer helices (M1, M3, M4) and the intra- and extracellular domain from our model. For a model of the α7 nAChR we showed that the barriers in a continuum electrostatic free energy profile almost doubled once the ligand binding domain and the outer TM helices were added to the M2 bundle [77], essentially due to an expansion of the low dielectric environment experienced by the ion. Because we are primarily interested in pinpointing the gate, the absolute value of the PMF (which is needed for accurate g_{max} estimates) is less important than the shape and relative heights. The latter will be less affected by uniformly applied corrections such as the ones discussed above, so that we will still be able to relate the peaks in the PMF to the residues responsible for the barrier. (It is still necessary to compute the PMF with all-atom simulations with explicit solvent and correct long range electrostatics as this is the only method that accounts for all effects (except for polarizability) that are important in confined geometries [17, 63].)

3.3. Sensitivity analysis

We have tested the sensitivity of the fundamental result, namely that the L251–V255–V259 side chain rings produce a hydrophobic gate in the closed state of the nAChR channel, to a number of factors. The profiles presented in figure 7(*A*) were calculated using the OPLS all-atom forcefield [51]. We have repeated the umbrella sampling simulations with the united-atom GROMOS96 forcefield [52] (figure 8): the PMFs share the same qualitative features such as the peak of the barrier at αV255 but the absolute values shift. The Na^+ peak height reduces to about $7kT$ and the barrier at the lower constriction site becomes more pronounced. The united-atom Cl^- PMF is higher than the all-atom one (about $10kT$). Consequently, the g_{max} estimates (equation 2) differ substantially as shown in table 1. The sensitivity of PMFs to the force field has also been noted in the case of gA [45, 47].

Our calculations are based on a medium-resolution cryo-EM derived model [2]. Thus the coordinates of the M2 helix bundle are not known with the same precision as from e.g. an x-ray structure. However, based on the simulations by Hung *et al* [55], relaxing the TM2 structure results in a pore with a radius >2.5 Å so even though the resolution is only 4 Å, the pore (of radius about 3 Å) is most likely not an artifact of

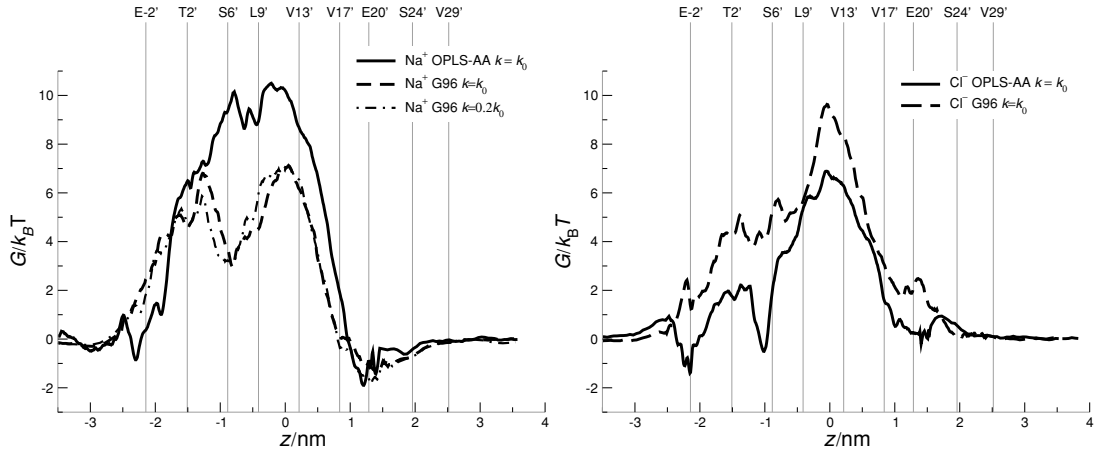

Figure 8. Sensitivity analysis of the PMF. *Left*: the PMF for Na^+ for the OPLS-AA and the GROMOS96 (G96) force fields (the latter for differing strengths of the backbone restraints force constant k; see the text). *Right*: the PMF for Cl^- ions. In all cases the umbrella-sampled and WHAM-unbiased PMF was matched up with the PMF derived from equilibrium simulations.

the lower resolution and it is always wide enough to admit an ion without physical occlusion. In the cryo-EM model, pore lining residues only interact with the solvent in the pore and their M2 neighbors (as the M2 bundle sits rather loosely in the outer M1/M3/M4 scaffold). Thus, from the perspective of our simulations, restraining the backbone atoms should be sufficient to enable sidechains to relax into their most favorable positions.

To assess the influence of the backbone restraints we also calculated the Na^+ PMF based on simulations with a $5\times$ weaker restraint on the M2 backbone atoms, thus allowing for an enhanced degree of protein flexibility (GROMOS96 forcefield). The root mean square deviation (RMSD) of the backbone atoms, averaged over 80 ns of simulation, is 0.653 ± 0.029 Å for the weaker restraints compared to 0.388 ± 0.014 Å for the standard restraints. The RMSD of the side chain atoms is 2.16 ± 0.07 Å (weak restraints) and 2.48 ± 0.11 Å, which is of the same magnitude as the side chain RMSD between the weak and standard restraint simulations (2.05 Å), i.e. in both simulations the sidechains are free to explore a similar range of conformations. We observed no significant change in the shape of the PMF (figure 8) and the conductances are reasonably similar (table 1).

We have also investigated the robustness of our results against small changes in the structural model of the nAChR pore domain. Thus, previous preliminary calculations of a Na^+ ion PMF for the M2 bundle of a homology model of the chick $\alpha 7$ nAChR [77] yielded a barrier of height between 8 and 12 kT distributed along the entire TM pore region with $g_{\max} = 0.02$ pS.

Thus the qualitative features of the Na^+ PMF are robust against small changes in sequence and in atomic coordinates. This is an important consideration given the resolution upon which the calculations are based. The Cl^- PMF differs more noticeably between the two force fields, which might indicate some subtle difference in how solvation effects in confined geometries are treated differently by an all-atom force field (OPLS-AA) versus an united-atom one (GROMOS96). Allen *et al* [45] compared an all-atom force field (CHARMM PARAM27) and a united-atom force field (GROMACS) for PMF calculations of the gA channel. This study (in conjunction with subsequent ones [46, 47]) seems to indicate that all-atom force fields are more successful at describing ion permeation in gA. Apparently, the same conclusion also holds for nAChR.

3.4. Comparison with experimental data

All the preceding results are based on the assumption that the structure of the transmembrane domain of nAChR [2] faithfully represents the closed state. In fact, nAChR and the other LGIC do not only have one closed (resting) state but also a closed desensitized state [78] and Karlin and coworkers find that the gate is in different positions in these two closed states [28, 29]. The cryo-EM images were taken in the absence of ACh [2] so the EM structure is likely to represent the closed resting state as desensitization requires prolonged exposure to agonist; such exposure to the agonist analog carbamylcholine resulted in low resolution structures different from the presumed resting-closed state [79]. All EM images were taken from tubular 2D crystals, which retain the physiological environment of the receptor: lipid composition and packing of receptors are close to the situation in the postsynaptic membrane of the muscle-derived electric organ of the *Torpedo* ray and the curvature of the tubular crystals is similar to the one of the folds in the neuromuscular junction [2, 80–82]. In addition, the channel in those 2D crystals could be rapidly converted to the open state through the application of the agonist ACh [81], which requires that the initial state was the resting-closed state [37]. Hence it appears unlikely that the cryo-EM structure represents a desensitized or other un-physiological states of the receptor. The resolution of the structure is not very high at 4 Å—just good enough to trace the backbone with some confidence. But assuming that the backbone is correctly described, the MD simulations allow the side chains to re-arrange themselves. Because the PMF

is not sensitive to the strength of the backbone restraints it follows that the local pore environment, which is formed by the mobile side chains, assumes a conformation independent of the details of the backbone motions.

The Na^+ PMF (figure 7) shows a pronounced barrier of about 10.5 kT at the hydrophobic girdle (between αL251 = 9′ and αV255 = 13′) and results in a very small maximum single-channel conductance. Therefore, the hydrophobic girdle is identified with the hydrophobic gate of nAChR, as hypothesized by Unwin and colleagues [2, 83], who based their inference on the protein structure.

This finding disagrees with the results of Karlin and coworkers [22, 27–29] who predict the position of the (resting) gate at about αT244 = 2′, based on biochemical data (accessibility of substituted cysteines to small, positively charged, sulfhydryl-specific reagents such as methanethiosulphonates). However, using the same method in the closely related $5HT_{3A}$ receptor, Panicker *et al* [31] find evidence for a gate between residues 9′ and 13′, and further experiments indicate that the narrow constriction site near 2′ remains unchanged between the open and the closed state [84]—the very same region that Karlin *et al* [22, 27–29] identify as the gate. Thus, either the gate location varies between different members of the same superfamily of ligand gated ion channels, or the methodology is sensitive to other changes in receptor properties. Paas *et al* [30], using Zn^{2+} binding to engineered His metal binding sites, report evidence that they interpret as ruling out a hydrophobic gating mechanism.

The free energy profiles for Na^+ and Cl^- do not allow us to explain the results of experiments finding the gate near or below the 2′ position as we cannot simply extrapolate from monovalent ions to the reactive reagents such as Zn^{2+} or the methanethiosulphonates. Further simulations would be required to investigate how those reagents could penetrate the hydrophobic girdle in the closed state while being excluded by the narrow constriction near 2′. In addition, one would need to assess the influence of the mutations to Cys or His on the channel behavior. The major hurdle in computationally addressing these experiments in a similar manner as presented here is the design of force field parameters describing the reactive reagents in a satisfactory manner.

4. Conclusion and outlook

In summary, we have shown that the hydrophobic girdle at the center of the nAChR M2 pore (as given by the cryo-electron microscopy structure) acts as a hydrophobic gate. This is in line with recent equilibrium simulations by Corry [44] and our own previous preliminary results for the related α7 receptor [77]. However, it should be noted that the current work rather robustly quantifies the *free energy* barriers to ion permeation (i.e. it includes explicit entropic and solvation effects in addition to direct particle interactions) and assesses the influence of choices in the computational method, namely the force field and the setup of the M2 helix bundle. In trying to evaluate the hydrophobic gating hypothesis, it is important that a quantitative and robust procedure be employed. In particular, the accuracy of our calculations is limited only by accuracy of the force field (not by e.g. modeling the water inside the pore after water in the bulk state, which we know to be a poor approximation [64, 85]) and the structure of the channel. The cryo-EM structure [2] is the most accurate atomistic description of a LGIC that is presently available. Our results demonstrate that if the nicotinic receptor adopts a conformation as seen in the 4 Å structure then (1) it will block the flow of Na^+ ions, and (2) it will gate them at the hydrophobic girdle, and not at the lower constriction site.

The opening of the hydrophobic gate is the final step in the full gating transition, which involves binding of two ligands, communicating a conformational change to the transmembrane domain and movement of the M2 helices [2, 55, 86] so as to increase the pore radius from about 3 Å to probably not more than 6.5 Å, a radius sufficient to allow ion permeation through a hydrophobic pore [16]. Hydrophobic gates may be widespread in a number of ion channels, including K channels [41] and bacterial mechanosensitive channels [14], in addition to other members of the Cys-loop superfamily [1]. A hydrophobic girdle also appears to be present in the protein-conducting channel formed by SecY [87] and so may be a general feature of transmembrane pore proteins that are tightly gated.

Numerous studies have shown that mutations of the conserved leucine (9′, 13′) and valine residues (13′, 17′) to more polar residues such as serine or threonine affect gating [1, 25, 32, 33, 36]. The effect of these mutations tends to be an increase in the opening probability or in the mean open time, i.e. they affect the gating transition. Hence the effect of those mutations is more complicated than a simple increase of conductance of the closed state (an increase in the leakage current). A possible hypothesis is that the open state is stabilized by the presence of a solvent; protein structure is not independent of its environment, a fact well known in protein folding. In this picture, a gate made more polar by a mutation will more readily admit water and ions, biasing the receptor toward the open state and so easing the transition to the open state.

From a broader methodological perspective, our results demonstrate the utility of computational approaches to the interpretation of membrane protein structures. But they also point to the difficulties in obtaining quantitative output from those simulations. In the present work the total simulated time was about 1μs (more than one order of magnitude larger than what is currently routinely reported) but as the analysis with respect to different MD force fields showed, there is still some work to be done in order to use MD simulations as a quantitative bridge between structure and function (as seen in experiments).

Acknowledgments

Our thanks to all of our colleagues, in particular Nigel Unwin and Tom Woolf, for valuable discussions. This work was funded by the Wellcome Trust, Merton College, Oxford, and the EPSRC (via the Bionanotechnology IRC).

Glossary

Free energy. A thermodynamic quantity of a system, which is minimal when the system is in equilibrium. It is crucial for a quantitative understanding of any physical system.

Gating, selectivity, conductance. The three characteristics of ion channels [13]. Gating refers to controlling the flow of ions through the channel; selectivity measures by how much one ion is more likely to permeate than an other; conductance describes the ease of flow of ions through the channel.

Ligand gated ion channels, LGIC. A class of ion channels that are activated by small molecular ligands such as acetylcholine or serotonin. They are primarily involved in functions of the nervous system. The gamma-aminobutyric acid type A ($GABA_A$), nicotinic acetylcholine (ACh), glycine and the serotonin (5-hydroxytryptamine, $5HT_3$) receptors form a superfamily with a common pentameric architecture [1].

Molecular dynamics simulation. Atoms are modeled as classical particles, moving according to Newton's equations of motions $\mathbf{F}_i = m_i \frac{\mathrm{d}^2\mathbf{x}_i}{\mathrm{d}t^2}$, which are integrated numerically with a small time step of typically 2×10^{-15} s. The forces are derived as $\mathbf{F}_i = -\frac{\mathrm{d}U}{\mathrm{d}\mathbf{x}_i}$ from a classical force field U [88]. The output of a simulation is an atomically-detailed 'movie' of the system.

Potential of mean force, PMF. A concept introduced by Kirkwood [89]: the free energy of a system as a function of a (externally constrained) reaction coordinate [63]. If the reaction coordinate is one dimensional (such as z along a channel pore) the PMF is called the 'free energy profile'. Derived from the constrained (configurational) partition function $Z(\xi) \propto \int \mathrm{d}^{3N}x \exp[-U(x)/kT]\delta[\xi - \xi(x)]$, the PMF along ξ is $\mathcal{W}(\xi) = -kT \ln Z(\xi)$ [90].

References

[1] Lester H A, Dibas M I, Dahan D S, Leite J F and Dougherty D A 2004 Cys-loop receptors: new twists and turns *Trends Neurosci.* **27** 329–36

[2] Miyazawa A, Fujiyoshi Y and Unwin N 2003 Structure and gating mechanism of the acetylcholine receptor pore *Nature* **423** 949–55

[3] Unwin N 2005 Refined structure of the nicotinic acetylcholine receptor at 4 Å resolution *J. Mol. Biol.* **346** 967–89

[4] Brejc K, van Dijk W J, Klaassen R V, Schuurmans M, van der Oost J, Smit A B and Sixma T K 2001 Crystal structure of an ACh-binding protein reveals the ligand-binding domain of nicotinic receptors *Nature* **411** 269–76

[5] Kuo A, Gulbis J M, Antcliff J F, Rahman T, Lowe E D, Zimmer J, Cuthbertson J, Ashcroft F M, Ezaki T and Doyle D A 2003 Crystal structure of the potassium channel KirBac1.1 in the closed state *Science* **300** 1922–6

[6] Zhou Y, Morais-Cabral J H, Kaufman A and MacKinnon R 2001 Chemistry of ion coordination and hydration revealed by a K^+ channel-Fab complex at 2.0 Å resolution *Nature* **414** 43–8

[7] Smart O S, Neduvelil J G, Wang X, Wallace B A and Sansom M S P 1996 HOLE: a program for the analysis of the pore dimensions of ion channel structural models *J. Mol. Graph.* **14** 354–360 http://hole.biop.ox.ac.uk/hole

[8] Humphrey W, Dalke A and Schulten K 1996 VMD—visual molecular dynamics *J. Mol. Graph.* **14** 33–8 http://www.ks.uiuc.edu/Research/vmd/

[9] Merritt E A and Bacon D J 1997 RASTER3D: photorealistic molecular graphics *Methods Enzymol.* **277** 505–24 http://www.bmsc.washington.edu/raster3d/raster3d.html

[10] White B H and Cohen J B 1992 Agonist-induced changes in the structure of the acetylcholine receptor M2 regions revealed by photoincorporation of an uncharged nicotinic noncompetitive antagonist *J. Biol. Chem.* **267** 15770–83

[11] Unwin N 1995 Acetylcholine-receptor channel imaged in the open state *Nature* **373** 37–43

[12] Chung S H, Hoyles M, Allen T and Kuyucak S 1998 Study of ionic currents across a model membrane channel using Brownian dynamics *Biophys. J.* **75** 793–809

[13] Hille B 2001 *Ion Channels of Excitable Membranes* 3rd edn (Sunderland, MA: Sinauer Associates)

[14] Moe P C, Levin G and Blount P 2000 Correlating a protein structure with function of a bacterial mechanosensitive channel *J. Biol. Chem.* **275** 31121–7

[15] Beckstein O, Biggin P C and Sansom M S P 2001 A hydrophobic gating mechanism for nanopores *J. Phys. Chem.* B **105** 12902–5

[16] Beckstein O and Sansom M S P 2004 The influence of geometry, surface character, and flexibility on the permeation of ions and water through biological pores *Phys. Biol.* **1** 42–52

[17] Beckstein O, Tai K and Sansom M S P 2004 Not ions alone: barriers to ion permeation in nanopores and channels *J. Am. Chem. Soc.* **126** 14694–5

[18] Schmid R, Miah A M and Sapunov V N 2000 A new table of the thermodynamic quantities of ionic hydration: values and some applications (enthalpy–entropy compensation and Born radii) *Phys. Chem. Chem. Phys.* **2** 97–102

[19] Bernèche S and Roux B 2001 Energetics of ion conduction through the K^+ channel *Nature* **414** 73–7

[20] Schneider T D and Stephens R M 1990 Sequence logos: a new way to display consensus sequences *Nucleic Acids Res.* **18** 6097–6100 http://www.ccrnp.ncifcrf.gov/~toms/logoprograms.html

[21] Bertrand D, Galzi J L, Devillers-Thiéry A, Bertrand S and Changeux J P 1993 Stratification of the channel domain in neurotransmitter receptors *Curr. Opin. Cell Biol.* **5** 688–93

[22] Karlin A 2002 Emerging structure of the nicotinic acetylcholine receptors *Nature Rev. Neurosci.* **3** 102–14

[23] Lester H A 1992 The permeation pathway of neurotransmitter-gated ion channels *Ann. Rev. Biophys. Biomol. Struct.* **21** 267–92

[24] Galzi J L and Changeux J P 1994 Neurotransmitter-gated ion channels as unconventional allosteric proteins *Curr. Opin. Struct. Biol.* **4** 554–65

[25] Labarca C, Nowak M W, Zhang H Y, Tang L X, Deshpande P and Lester H A 1995 Channel gating governed symmetrically by conserved leucine residues in the M2 domain of nicotinic receptors *Nature* **376** 514–6

[26] Tasneem A, Iyer L M, Jakobsson E and Aravind L 2005 Identification of the prokaryotic ligand-gated ion channels and their implications for the mechanisms and origins of animal cys-loop ion channels *Genome Biol.* **6** R4

[27] Akabas M H, Kaufmann C, Archdeacon P and Karlin A 1994 Identification of acetylcholine receptor channel-lining residues in the entire M2 segment of the α subunit *Neuron* **13** 919–27

[28] Wilson G G and Karlin A 1998 The location of the gate in the acetylcholine receptor channel *Neuron* **20** 1269–81

[29] Wilson G G and Karlin A 2001 Acetylcholine receptor channel structure in the resting, open, and desensitized states probed

with the substituted-cysteine-accessibility method *Proc. Natl Acad. Sci. USA* **98** 1241–8
[30] Paas Y, Gibor G, Grailhe R, Savatier-Duclert N, Dufresne V, Sunesen M, de Carvalho L P, Changeux J P and Attali B 2005 Pore conformations and gating mechanism of a cys-loop receptor *Proc. Natl Acad. Sci. USA* **102** 15877–82
[31] Panicker S, Cruz H, Arrabit C and Slesinger P A 2002 Evidence for a centrally located gate in the pore of a serotonin-gated ion channel *J. Neurosci.* **22** 1629–39
[32] Revah F, Bertrand D, Galzi J L, Devillers-Thiéry A, Mulle C, Hussy N, Bertrand S, Ballivet M and Changeux J P 1991 Mutations in the channels domain alter desensitization of a neuronal nicotinic receptor *Nature* **353** 846–9
[33] Filatov G N and White M M 1995 The role of conserved leucines in the M2 domain of the acetylcholine-receptor in channel gating *Molecul. Pharmacol.* **48** 379–84
[34] England P M, Zhang Y, Dougherty D A and Lester H A 1999 Backbone mutations in transmembrane domains of a ligand-gated ion channel *Cell* **96** 89–98
[35] Horenstein J, Wagner D A, Czajkowski C and Akabas M H 2001 Protein mobility and GABA-induced conformational changes in $GABA_A$ receptor pore-lining M2 segment *Nature Neurosci.* **4** 477–85
[36] Plazas P V, Rosa M J D, Gomez-Casati M E, Verbitsky M, Weisstaub N, Katz E, Bouzat C and Elgoyhen A B 2005 Key roles of hydrophobic rings of TM2 in gating of the $\alpha 9\alpha 10$ nicotinic cholinergic receptor *Brit. J. Pharmacol.* **145** 963–74
[37] Changeux J P and Edelstein S J 1998 Allosteric receptors after 30 years *Neuron* **21** 959–80
[38] Anishkin A and Sukharev S 2004 Water dynamics and dewetting transitions in the small mechanosensitive channel MscS *Biophys. J.* **86** 2883–95
[39] Bass R B, Strop P, Barclay M and Rees D C 2002 Crystal structure of *Escherichia coli* MscS, a voltage-modulated and mechanosensitive channel *Science* **298** 1582–7
[40] Spronk S A, Elmore D E and Dougherty D A 2006 Voltage-dependent hydration and conduction properties of the hydrophobic pore of the mechanosensitive channel of small conductance *Biophys. J.* **90** 3555–69
[41] Roux B, Bernèche S and Im W 2000 Ion channels, permeation, and electrostatics: insight into the function of KcsA *Biochemistry* **39** 13295–306
[42] Jogini V and Roux B 2005 Electrostatics of the intracellular vestibule of K^+ channels *J. Mol. Biol.* **354** 272–88
[43] Corry B 2004 Theoretical conformation of the closed and open states of the acetylcholine receptor channel *Biochim. Biophys. Acta* **1663** 2–5
[44] Corry B 2006 An energy efficient gating mechanism in the acetylcholine receptor channel suggested by molecular and Brownian dynamics *Biophys. J.* **90** 799–810
[45] Allen T W, Baştuğ T, Kuyucak S and Chung S H 2003 Gramicidin A channel as a test ground for molecular dynamics force fields *Biophys. J.* **84** 2159–68
[46] Allen T W, Andersen O S and Roux B 2004 Energetics of ion conduction through the gramicidin channel *Proc. Natl Acad. Sci. USA* **101** 117–22
[47] Allen T W, Andersen O S and Roux B 2006 Ion permeation through a narrow channel: using gramicidin to ascertain all-atom molecular dynamics potential of mean force methodology and biomolecular force fields *Biophys. J.* **90** 3447–68
[48] Vriend G 1990 WHATIF: a molecular modeling and drug design program *J. Mol. Graph.* **8** 52–6 http://www.cmbi.kun.nl/whatif/
[49] Nielsen J E and Vriend G 2001 Optimizing the hydrogen-bond network in Poisson–Boltzmann equation-based pKa calculations *Proteins: Struct. Funct. Genet.* **43** 403–12
[50] Rocchia W, Alexov E and Honig B 2001 Extending the applicability of the nonlinear Poisson–Boltzmann equation: multiple dielectric constants and multivalent ions *J. Phys. Chem. B* **105** 6507–14 http://trantor.bioc.columbia.edu/delphi/
[51] Kaminski G A, Friesner R A, Tirado-Rives J and Jorgensen W L 2001 Evaluation and reparametrization of the OPLS-AA force field for proteins via comparison with accurate quantum chemical calculations on peptides *J. Phys. Chem. B* **105** 6474–87
[52] van Gunsteren W F, Billeter S R, Elsing A A, Hünenberger P H, Krüger P, Mark A E, Scott W R P and Tironi I G 1996 *Biomolecular Simulation: The GROMOS96 Manual and User Guide* (Zürich and Groningen: Biomos and Hochschulverlag AG an der ETH Zürich)
[53] Berweger C D, van Gunsteren W F and Müller-Plathe F 1995 Force field parametrization by weak coupling: re-engineering SPC water *Chem. Phys. Lett.* **232** 429–36
[54] Åqvist J 1990 Ion-water interaction potentials derived from free energy perturbation simulations *J. Phys. Chem.* **94** 8021–4
[55] Hung A, Tai K and Sansom M S P 2005 Molecular dynamics simulation of the M2 helices within the nicotinic acetylcholine receptor transmembrane domain: structure and collective motions *Biophys. J.* **88** 3321–33
[56] Lindahl E, Hess B and van der Spoel D 2001 Gromacs 3.0: a package for molecular simulation and trajectory analysis *J. Mol. Mod.* **7** 306–17 http://www.gromacs.org
[57] Darden T, York D and Pedersen L 1993 Particle mesh Ewald—an $N \log(N)$ method for Ewald sums in large systems *J. Chem. Phys.* **98** 10089–92
[58] Hess B, Bekker H, Berendsen H J C and Fraaije J G E M 1997 LINCS: a linear constraint solver for molecular simulations *J. Comp. Chem.* **18** 1463–72
[59] Miyamoto S and Kollman P A 1992 SETTLE: an analytical version of the SHAKE and RATTLE algorithms for rigid water models *J. Comp. Chem.* **13** 952–62
[60] Torrie G M and Valleau J P 1977 Nonphysical sampling distributions in Monte Carlo free-energy estimation: umbrella sampling *J. Comp. Phys.* **23** 187–99
[61] Valleau J P and Torrie G M 1977 A guide to Monte Carlo for statistical mechanics: 2. Byways *Statistical Mechanics. Part A: Equilibrium Techniques* ed B J Berne *(Modern Theoretical Chemistry)* vol 5 (New York: Plenum) chapter 5, pp 169–194
[62] Kumar S, Bouzida D, Swendsen R H, Kollman P A and Rosenberg J M 1992 The weighted histogram analysis method for free-energy calculations on biomolecules. I. The method *J. Comp. Chem.* **13** 1011–21
[63] Roux B, Allen T, Bernèche S and Im W 2004 Theoretical and computational models of biological ion channels *Q. Rev. Biophys.* **37** 15–103
[64] Beckstein O and Sansom M S P 2003 Liquid-vapor oscillations of water in hydrophobic nanopores *Proc. Natl Acad. Sci. USA* **100** 7063–8
[65] Tieleman D P, Biggin P C, Smith G R and Sansom M S P 2001 Simulation approaches to ion channel structure-function relationships *Q. Rev. Biophys.* **34** 473–561
[66] Bateman A *et al* 2004 The pfam protein families database *Nucleic Acids Res.* **32** D138–D141 http://www.sanger.ac.uk/Software/Pfam/
[67] Thompson J D, Higgins D G and Gibson T J 1994 CLUSTALW: improving the sensitivity of progressive multiple sequence alignment through sequence weighting, position-specific gap penalties and weight matrix choice *Nucleic Acids Res.* **22** 4673–780
[68] Clamp M, Cuff J, Searle S M and Barton G J 2004 The JALVIEW Java alignment editor *Bioinformatics* **20** 426–7 http://www.jalview.org

[69] Sotomayor M and Schulten K 2004 Molecular dynamics study of gating in the mechanosensitive channel of small conductance MscS *Biophys. J.* **87** 3050–65
[70] Chiu S W, Subramaniam S and Jakobsson E 1999 Simulation study of a gramicidin/lipid bilayer system in excess water and lipid: II. Rates and mechanisms of water transport *Biophys. J.* **76** 1939–50
[71] Corry B, Kuyucak S and Chung S H 2000 Invalidity of continuum theories of electrolytes in nanopores *Chem. Phys. Lett.* **320** 35–41
[72] Imoto K, Busch C, Sakmann B, Mishina M, Konno T, Nakai J, Bujo H, Mori Y, Fukuda K and Numa S 1988 Rings of negatively charged amino acids determine the acetylcholine receptor channel conductance *Nature* **335** 645–8
[73] Galzi J L, Devillers-Thiéry A, Hussy N, Bertrand S, Changeux J P and Bertrand D 1992 Mutations in the channel domain of a neuronal nicotinic receptor convert ion selectivity from cationic to anionic *Nature* **359** 500–5
[74] Corringer P J, Le Novère N and Changeux J P 2000 Nicotinic receptors at the amino acid level *Annu. Rev. Pharmacol. Toxicol.* **40** 431–58
[75] Gunthorpe M J and Lummis S C R 2001 Conversion of the ion selectivity of the 5-HT_{3A} receptor from cationic to anionic reveals a conserved feature of the ligandgated ion channel superfamily *J. Biol. Chem.* **276** 10977–83
[76] Wang F and Imoto K 1992 Pore size and negative charge as structural determinants of permeability in the torpedo nicotinic acetylcholine receptor channel *Proc. R. Soc.* B **250** 11–7
[77] Amiri S, Tai K, Beckstein O, Biggin P C and Sansom M S P 2005 The α7 nicotinic acetylcholine receptor: molecular modelling, electrostatics and energetics of permeation *Molec. Membr. Biol.* **22** 151–62
[78] Katz B and Thesleff S 1957 A study of 'desensitisation' produced by acetylcholine at the motor end-plate *J. Physiol.* **138** 63–80
[79] Unwin N, Toyoshima C and Kubalek E 1988 Arrangement of the acetylcholine receptor subunits in the resting and desensitized states, determined by cryoelectron microscopy of crystallized Torpedo postsynaptic membranes *J. Cell Biol.* **107** 1123–38
[80] Unwin N 1993 Nicotinic acetylcholine-receptor at 9 Å resolution *J. Mol. Biol.* **229** 1101–24
[81] Unwin N 1995 Acetylcholine-receptor channel imaged in the open state *Nature* **373** 37–43
[82] Unwin N 2000 The Croonian lecture 2000. Nicotinic acetylcholine receptor and the structural basis of fast synaptic transmission *Phil. Trans. R. Soc.* B **355** 1813–29
[83] Unwin N 2003 Structure and action of the nicotinic acetylcholine receptor explored by electron microscopy *FEBS Lett.* **555** 91–5
[84] Panicker S, Cruz H, Arrabit C, Suen K F and Slesinger P A 2004 Minimal structural rearrangement of the cytoplasmic pore during activation of the 5-HT_{3A} receptor *J. Biol. Chem.* **279** 28149–58
[85] Hummer G, Rasaiah J C and Noworyta J P 2001 Water conduction through the hydrophobic channel of a carbon nanotube *Nature* **414** 188–90
[86] Grosman C, Zhou M and Auerbach A 2000 Mapping the conformational wave of acetylcholine receptor channel gating *Nature* **403** 773–6
[87] Van den Berg B, Clemons W M, Collinson I, Modis Y, Hartmann E, Harrison S C and Rapoport T A 2004 X-ray structure of a protein-conducting channel *Nature* **427** 36–44
[88] Frenkel D and Smit B 2002 *Understanding Molecular Simulations* 2nd edn (San Diego, CA: Academic)
[89] Kirkwood J G 1935 Statistical mechanism of fluid mixtures *J. Chem. Phys.* **3** 300–13
[90] Chaikin P M and Lubensky T C 2000 *Principles of Condensed Matter Physics* (Cambridge: Cambridge University Press)